Invited Paper

Toward quantum information processing using EIT in diamond

Charles Santori[a], David Fattal[a], Sean M. Spillane[a], Marco Fiorentino[a], R. G. Beausoleil[b,†], W. J. Munro[c], T. P. Spiller[c], Andrew D. Greentree[d,f], Paolo Olivero[f], Martin Draganski[g], James R. Rabeau[f], Patrick Reichart[f], Brant C. Gibson[e,f], Sergey Rubanov[d,f], Shane T. Huntington[d,f], David N. Jamieson[d,f], and Steven Prawer[d,f]

[a]Hewlett-Packard Laboratories, 1501 Page Mill Rd., Palo Alto, CA 94304, USA;
[b]Hewlett-Packard Laboratories, 13837 175th Pl. NE, Redmond, WA 98052-2180, USA;
[c]Hewlett-Packard Laboratories, Filton Road Stoke Gifford, Bristol BS34 8QZ, UK;
[d]Centre for Quantum Computer Technology;
[e]Quantum Communications Victoria;
[f]School of Physics, The University of Melbourne, Melbourne, Victoria 3010, Australia;
[g]Applied Physics, RMIT University, GPO Box 2476V, Melbourne, Victoria 3001, Australia;

ABSTRACT

We describe how a quantum non-demolition device based on electromagnetically-induced transparency in solid-state atom-like systems could be realized. Such a resource, requiring only weak optical nonlinearities, could potentially enable photonic quantum information processing (QIP) that is much more efficient than QIP based on linear optics alone. As an example, we show how a parity gate could be constructed. A particularly interesting physical system for constructing devices is the nitrogen-vacancy defect in diamond, but the excited-state structure for this system is unclear in the existing literature. We include some of our latest spectroscopic results that indicate that the optical transitions are generally not spin-preserving, even at zero magnetic field, which allows the realization of a Λ-type system.

Keywords: Quantum information processing, electromagnetically induced transparency, nonlinear optics, diamond, nitrogen-vacancy

1. INTRODUCTION

The search for devices that exploit quantum coherence in non-trivial fashions has rapidly become one of the major technological challenges of the twenty-first century. This search has as its goals devices ranging in complexity from single photon sources to massively entangled quantum computers. Tied to the technological imperatives are the theoretical underpinnings of a new understanding of quantum mechanics: quantum information processing (QIP), and the quest to build new devices is closely linked to the desire to fully understand the new, and often surprising, possibilities afforded by entangled quantum systems.

For QIP applications, photon-based implementations have a privileged place. As individual quantum systems, photons are perhaps the easiest to manipulate, and without internal structure, superposition states of, for example, polarization states or modes in an interferometer, can be maintained with negligible decoherence. Hence they are ideal candidates for qubits (two-state quantum systems). Historically, one of the first suggestions for an implementation of a two-qubit gate was in an optical system, exhibiting a large lossless Kerr-type nonlinearity.[1] However this (and related) schemes require a nonlinearity sufficient to impart a $\pi/2$ phase shift, for an intensity change of a single photon without any photon absorption. While this is in principle possible for devices based on single emitters coupled to microcavities, such a large single-photon nonlinear phase shift has not yet been realized experimentally in these systems. Non-deterministic schemes, typified by the KLM scheme[2] present another way to realize scalable quantum computing, although the extra overhead in terms of the number of photons used per gate may be undesirable.

† E-mail: ray.beausoleil@hp.com

Advanced Optical and Quantum Memories and Computing III, edited by Hans J. Coufal, Zameer U. Hasan, Alan E. Craig, Proc. of SPIE Vol. 6130, 613005, (2006) · 0277-786X/06/$15 · doi: 10.1117/12.660189

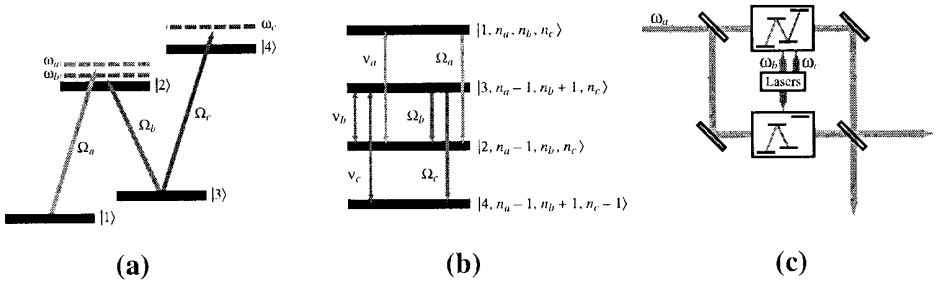

Figure 1. Electric dipole interaction between a four-state $\mathcal{N}$ atom and a nearly resonant three-frequency electromagnetic field. (a) In the semiclassical view, two atomic states are separated by the energy $\hbar\omega_{ij}$, and coupled by a classical field oscillating at the frequency $\omega_k = \omega_{ij} + \nu_k$. The strength and phase of the corresponding dipole interaction is represented by the Rabi frequency $\Omega_k \propto \sqrt{n_k}$. (b) In the quantum view, the states of the atom + photons system separate into manifolds coupled internally by resonant transitions. (c) A model Mach-Zehnder interferometer illustrating an architecture for a "dual rail" quantum phase-shifter using four-state $\mathcal{N}$ atoms. The upper arm is denoted by "1" and the lower arm by "0."

An alternative approach is to use systems exhibiting a weak, lossless nonlinearity, and to use homodyne measurement of a *strong* probe field to effectively magnify the resultant nonlinearity, and realize a quantum non-demolition (QND) measurement of an unknown field, representing the qubit. This application (discussed below) forms the context for the present work.

Nitrogen-vacancy (N-V) centers in diamond have attracted much interest in the field of quantum information because they have long-lived electronic spin levels coupled to moderately strong optical transitions. For example, optical readout of the electronic spin of a single N-V center has been reported[3] as well as the ability to control the coupling between spins of electrons and nuclei.[4] These results have led to proposals for quantum-information applications including single photon sources,[5–7] quantum memories and repeaters,[8] quantum computation using electron spins controlled by microwave fields,[9] and quantum computation based on all-optical manipulation of electron spins.[10] Methods of fabrication of monolithic, microstructured diamond containing N-V centers, suitable for QIP applications has been reported,[11] and diamond as a matrix for QIP has been recently reviewed.[12] Here, we investigate the feasibility of using diamond N-V centers for nonlinear optics and quantum non-demolition measurement at the single-photon level.

Nonlinear-optical devices based on EIT, as well as all-optical manipulation of electron spin, requires two ground states to be connected to a common excited state by optical transitions. However, in N-V diamond, it is not clear from the existing literature how to realize this. Recently it has been widely believed[9] that the optical transitions between the ${}^3A$ ground states and ${}^3E$ excited states are almost perfectly spin-preserving. This is convenient for optical readout of the spin state of an N-V center, since many fluorescence cycles may be excited without changing the spin state, but this would preclude the possibility of obtaining a Λ system. To solve this problem, it has been proposed that a Λ system could be obtained by applying a particular magnetic field of approximately 0.1 T, close to an anticrossing between the $m_s = -1$ and $m_s = 0$ ground states. Close to this anticrossing, the eigenstates are linear combinations of $m_s = -1$ and $m_s = 0$ that each couple to the same pair of excited states. This technique was used in Ref. 13 where an EIT effect was reported.

2. APPLICATIONS OF EIT TO QUANTUM INFORMATION PROCESSING

In previous work,[14,15] we considered a model of the nonlinear electric dipole interaction between three quantum electromagnetic radiation fields with angular frequencies ω_a, ω_b, and ω_c and a corresponding four-state atomic system in the $\mathcal{N}$ configuration, as shown in Fig. 1(a). We considered a fixed number, N, of atoms, that are stationary in a volume small compared to the optical wavelengths, and we assumed that the three frequency channels of the resonant four-state manifold of the resulting quantum system shown in Fig. 1(b) are driven by Fock states containing n_a, n_b, and n_c photons, with corresponding Rabi frequencies Ω_a, Ω_b, and Ω_c, respectively. As an example of the use of an EIT system as a phase-shifter, we incorporate the atomic system into the dual-rail

Mach-Zehnder interferometer shown in Fig. 1(c). Our measurement result is a phase shift to the photon in mode a on the upper rail, conditioned on the presence of one or more photons in mode c, which represents the unknown qubit state. Mode b is used to create the necessary EIT nonlinearity in the Λ or $\mathcal{N}$ configuration. In one arm of the interferometer, the four-state atoms are prepared using $\Omega_c \neq 0$ to provide a phase shift at the probe frequency ω_a while remaining largely transparent and dispersive. In the second arm, $\Omega_c = 0$, and the system is tuned to match the absorption and dispersion provided by the atoms in the first arm, allowing the interferometer to remain time-synchronous.

2.1. SINGLE-PHOTON QND DETECTOR

We have proposed[16] an implementation of the quantum non-demolition (QND) single-photon detection scheme originally described by Imoto, Haus and Yamamoto,[17] with the required optical nonlinearity provided by the giant Kerr effect achievable with AC Stark-shifted electromagnetically induced transparency (EIT).[18,19] In a QND measurement, the signal photons are not destroyed and can be reused if required.[20]

The photon number QND measurement is in principle achieved using a simple cross-Kerr nonlinearity[17,21] given by

$$H_{\text{Kerr}} = \hbar\tilde{W}\, a^\dagger a\, c^\dagger c \tag{1}$$

Here the QND signal (probe) mode has the creation and destruction operators given by $a^\dagger, a$ ($c^\dagger, c$) respectively. If the signal field contains n_a photons and the probe field is in an initial coherent state with amplitude α_c, the cross-Kerr optical nonlinearity causes the combined system to evolve as

$$|\Psi(t)\rangle_{out} = e^{-i\tilde{W}t a^\dagger a c^\dagger c}|n_a\rangle|\alpha_c\rangle = |n_a\rangle|\alpha_c e^{-in_a\tilde{W}t}\rangle. \tag{2}$$

The Fock state $|n_a\rangle$ is unaffected by the interaction, but the coherent state $|\alpha_c\rangle$ picks up a phase shift directly proportional to the number of photons n_a in the $|n_a\rangle$ state. If we measure this phase shift using a homodyne measurement (depicted schematically in Fig. 2), we can infer the number of photons in the signal mode a. The homodyne apparatus allows measurement of the quadrature operator which we define as $\hat{x}(\phi) \equiv ce^{i\phi} + c^\dagger e^{-i\phi}$, with an expected result $\langle\hat{x}(\phi)\rangle = 2\text{Re}\,[\alpha_c]\cos\delta + 2\text{Im}\,[\alpha_c]\sin\delta$, where $\delta = -\phi + n_a\tilde{W}t$. For a real initial α_c, a highly efficient homodyne measurement of the momentum quadrature $Y \equiv \hat{x}(\pi/2)$ would yield the signal $\langle Y\rangle = 2\alpha_c\sin(n_a\tilde{W}t)$ with a variance of one, thus giving a signal-to-noise ratio of $\text{SNR}_Y = 2\alpha_c\sin(n_a\tilde{W}t)$. If the input in mode a is either the Fock state $|0\rangle$ or $|1\rangle$, the respective output states of the probe mode c are the coherent states $|\alpha_c\rangle$ or $|\alpha_c e^{-i\tilde{W}t}\rangle$. Using the momentum quadrature measurement, the probability of misidentifying one of these states for one another is then $P_{\text{error}} = \frac{1}{2}\text{erfc}(\text{SNR}_Y/2\sqrt{2})$. A signal-to-noise ratio of $\text{SNR}_Y = 4.6$ would thus give $P_{\text{error}} \sim 10^{-2}$. To achieve the necessary phase shift we require $\alpha_c\sin(\tilde{W}t) \approx 2.3$, which can be achieved in a number of ways dependent upon the range of values available for α_c and $\tilde{W}t$. For example, we could choose $\alpha_c \gg 2.3$ with $\tilde{W}t$ small and satisfy the above inequality; alternatively we could choose $\tilde{W}t = \pi/2$ with $\alpha_c = 2.3$. The particular regime chosen depends on the strength of the Kerr nonlinearity achievable in the physical system.

The discussion above assumes single-mode signal and probe fields, while in practice we will have input pulses that can become distorted or even entangled inside the nonlinear medium. The calculation in Ref. 16 does not include effects such as group-velocity mismatch between the signal and probe pulses or inhomoeneous broadening of the optical transitions, and thus part of our ongoing work is to determine whether these difficulties can be overcome.

2.2. TWO-PHOTON INTERACTIONS: A PARITY GATE

The single-photon QND detection ideas can be applied to several photonic qubits. Basically, to perform a more "generalized" type of measurement between different photonic qubits, the homodyne measurement could be delayed. The probe beam can then interact with several cross-Kerr non-linearities, where the signal photon mode is different in each interaction case. The probe beam measurement can then be made after all these interactions and—very importantly—be made in a collective way that could condition onto interesting two-photon states.[22] For example, a non-destructive detection can be made that distinguishes superpositions and mixtures of the states $|HH\rangle$ and $|VV\rangle$ from $|HV\rangle$ and $|VH\rangle$. The key here is that it is possible to arrange no

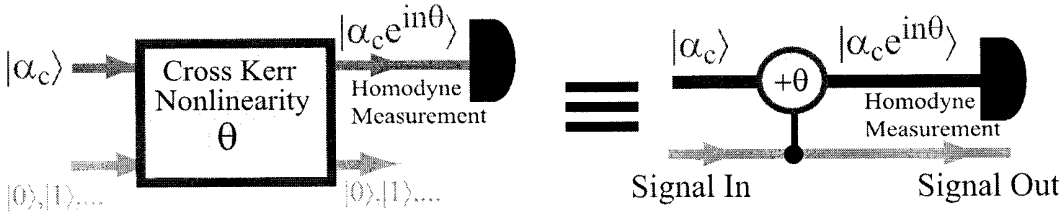

Figure 2. Schematic diagram of a photon number quantum non-demolition detector based on a cross-Kerr optical nonlinearity and a homodyne measurement.[17] The two inputs are a Fock state $|n_a\rangle$ (with $n_a = 0, 1, ..$) in the signal mode a and a coherent state with real amplitude α_c in the probe mode c. The presence of photons in mode a causes a phase shift on the coherent state $|\alpha_c\rangle$ directly proportional to n_a which can be determined with a momentum quadrature measurement.

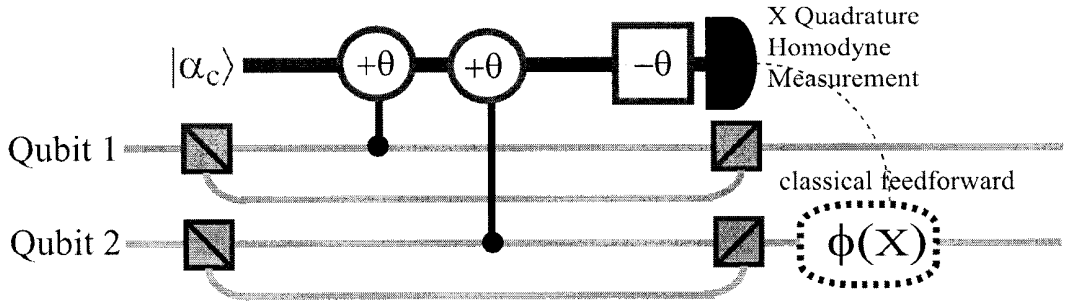

Figure 3. Schematic diagram of a two-qubit polarization QND gate that distinguishes superpositions and mixtures of the states $|HH\rangle$ and $|VV\rangle$ from $|HV\rangle$ and $|VH\rangle$ using two cross-Kerr non-linearities, a fixed phase shift $(-\theta)$ and a coherent laser probe beam $|\alpha_c\rangle$. Note that since the detuning ν_c of the coherent state determines the sign of the applied phase shift,[14, 15] obtaining phase shifts that are opposite in sign is not experimentally possible using EIT. We therefore employ two identical EIT interaction regions to apply equal positive phase shifts to both $|H\rangle$ modes, and then incorporate a linear phase delay of $-\theta$ into the homodyne measurement. The gate operates by splitting each polarization qubit into a "which path" qubit on a polarizing beam-splitter. The action of the cross-Kerr non-linearities is to put a phase shift θ on the probe beam only if a photon is present in that mode. After the non-linear interactions the "which path" qubit are converted back to polarization qubits. Including the fixed phase shift, the probe beam only picks up a phase shift if the states $|HH\rangle$ and/or $|VV\rangle$ were present and hence an appropriate homodyne measurement allows the states $|HH\rangle$ and $|VV\rangle$ to be distinguished from $|HV\rangle$ and $|VH\rangle$. The two-qubit polarization QND gate thus acts like a parity checking device. For an input state of $|HH\rangle + |HV\rangle + |VH\rangle + |VV\rangle$, the parity gate conditions on an X homodyne measurement either to the state $|HV\rangle + |VH\rangle$ or to $e^{i\phi(X)}|HH\rangle + e^{-i\phi(X)}|VV\rangle$ where $\phi(X)$ is a phase shift dependent on the exact result of the homodyne measurement. A simple phase shift achieved via classical feed-forward then allows this second state to be transformed.

net phase shift on the $|HV\rangle$ and $|VH\rangle$ terms while having a phase shift on the $|HH\rangle$ and $|VV\rangle$ terms. We call this generalization a *two-qubit polarization parity QND gate.*

We now discuss the operation of this parity QND gate, shown schematically in Fig. 3 in a configuration appropriate for EIT. Consider a general two-qubit state, written as $|\Psi_{12}\rangle = \beta_0|HV\rangle+\beta_1|HH\rangle+\beta_2|VV\rangle+\beta_3|VH\rangle$. As shown in Fig. 3, these qubits are individually split on polarizing beam-splitters (PBS) into spatially encoded qubits, which then interact with separate weak cross-Kerr non-linearities. The action of the PBS's and non-linearities evolves the combined system of photonic qubits and probe beam to

$$|\psi\rangle_T = [\beta_0|HV\rangle + \beta_3|VH\rangle]\,|\alpha_c\rangle_p + \beta_1|HH\rangle|\alpha_c e^{i\theta}\rangle_p + \beta_2|VV\rangle|\alpha_c e^{-i\theta}\rangle_p$$

It is now clear that the $|HV\rangle$ and $|VH\rangle$ terms pick up no net phase shift and remain coherent with respect to each other while the $|HH\rangle$ and $|VV\rangle$ pick up opposite sign phase shifts θ. This allows them to be distinguished by a general homodyne/heterodyne measurement. Such a measurement must not allow the sign of the phase shift to be determined. With α_c real, an X homodyne measurement (projecting onto $|X\rangle\langle X|$) conditions the two-qubit state to

$$\begin{aligned} |\psi_X\rangle_T = {} & f(X,\alpha_c)\,[\beta_0|HV\rangle + \beta_3|VH\rangle] \\ & + f(X,\alpha_c\cos\theta)\left[\beta_1 e^{i\phi(X)}|HH\rangle + \beta_2 e^{-i\phi(X)}|VV\rangle\right] \end{aligned} \tag{3}$$

where

$$f(x,\beta) = \exp\left[-\frac{1}{4}(x-2\beta)^2\right]/(2\pi)^{1/4} \tag{4}$$

$$\phi(x) = \alpha_c \sin\theta(x - 2\alpha_c\cos\theta) \quad [\mathrm{Mod}2\pi]\,. \tag{5}$$

Note that $f(X,\alpha_c)$ and $f(X,\alpha_c\cos\theta)$ are two Gaussian amplitudes with the mid point between the peaks located at $X_0 \equiv \alpha_c[1+\cos\theta]$ and the peaks separated by a distance $X_d \equiv 2\alpha_c[1-\cos\theta]$. As long as this difference is large ($X_d \sim \alpha_c\theta^2 \gg 1$), then there is little overlap between these amplitudes. For an X homodyne giving $X > X_0$ the state given by Eq. (3) is taken to collapse to

$$|\psi_{X>X_0}\rangle_T \sim \beta_0|HV\rangle + \beta_3|VH\rangle \tag{6}$$

whereas for $X < X_0$ it is taken to be

$$|\psi_{X<X_0}\rangle_T \sim \beta_1 e^{i\phi(X)}|HH\rangle + \beta_2 e^{-i\phi(X)}|VV\rangle \tag{7}$$

The action of this two-qubit polarization parity QND gate is now very clear; it splits the odd parity terms, $\{|HV\rangle, |VH\rangle\}$, given by Eq. (6) near-deterministically from the even parity states, $\{|HH\rangle, |VV\rangle\}$, given by Eq. (7). This demonstrates how to engineer strong non-linear interactions using only relatively weak cross-Kerr effects. Modification of the polarizations and relative couplings allows different nonlinear coupling arrangements, and there is no requirement for the discriminated states to have any symmetry.

Note also that in Eq. (7) the state depends on the value of the measured quadrature X. However, simple local rotations using phase shifters dependent on the measurement result X can be performed via a feed-forward process to transform this state to $\beta_1|H\rangle_a|H\rangle_b + \beta_2|V\rangle_a|V\rangle_b$ which is independent of X. This does mean that the homodyne measurement must be able to determine $\phi(X)$ accurately, since otherwise the unwanted phase factors cannot be undone. Thus the uncertainty in the X quadrature homodyne measurement must be much less than $2\pi/\alpha_c\sin\theta$. This can generally be achieved by ensuring that the strength of the local oscillator is much more intense than the probe mode.

In the odd and even parity states represented by Eq. (6) and Eq. (7), respectively, we have used the approximate symbol $\sim$, as there is a small but non-zero probability that the odd-parity state can occur for $X < X_0$, and vice versa. The probability of such an error occurring is given by

$$P_{\mathrm{error}} = \frac{1}{2}\left(1 - \mathrm{Erf}[X_d/2\sqrt{2}]\right)\,, \tag{8}$$

which is less than 10^{-4}, the generally accepted threshold for quantum error correction,[23] when the distance $X_d \sim \alpha_c\theta^2 > 6$. This shows that it is possible to achieve an effectively deterministic parity measurement operating in the regime of weak cross-Kerr non-linearities ($\theta \ll \pi$). The requirement here on $\alpha_c\theta^2$ is more difficult to satisfy than the corresponding requirement on $\alpha_c\theta$ discussed for the photon detector. However, alternative parity gates have been proposed that scale as $\alpha_c\theta$, described in Refs. 25, 27.

2.3. EXTENSIONS TO OTHER QUANTUM OPERATIONS

The idea of amplifying a weak optical Kerr nonlinearity using homodyne detection and feed-forward can be extended beyond quantum nondemolition and parity detection.[24,25] For example, using the two-photon parity gate as a primitive, a symmetry analyzer for nondestructive Bell-state measurement[22] and a CNOT gate[26] can (in principle) be constructed. It is not clear yet whether the required X homodyne measurement can be performed, but — by displacing the coherent probe state to the vacuum[27] — it is possible that QND may be used instead. Again we note, that combined with the fact that single qubit operations are easily performed with polarization optics in a photonic implementation to extremely high fidelity, the presence of any non-trivial coupling is sufficient for universal quantum computation.

3. SPECTROSCOPY OF DIAMOND NV CENTERS

Finally, we present some recent spectroscopic data that help to answer the question of whether N-V centers in diamond can provide a suitable level structure for nonlinear-optical devices. All-optical manipulation of electron spin requires a three-level Λ system, while the all-optical QND scheme described above calls for a four-level N system.

The N-V center in diamond has been studied extensively in bulk samples, but few studies have been performed on single N-V centers or small ensembles, the situation relevant for quantum information applications. Spectral hole-burning experiments in bulk N-V diamond were performed by Reddy, Manson *et al.* in Refs. 28, 29 at zero magnetic field. These studies resolved an antihole feature at ± 2.88 GHz which matches the crystal-field splitting between the $m_s = 0$ and $m_s = \pm 1$ ground states. This antihole feature cannot be explained if all of the optical transitions are spin-preserving. At least one of the excited states couples to multiple ground states, and it should be possible therefore to use N-V centers with this energy-level structure at zero magnetic field as Λ-type systems. The effect of strain on the excited state manifold has also been reported,[29,30] and it appears that the excited-state structure is highly sensitive to strain. The apparent contradictions in the literature regarding the excited-state structure need to be resolved before we can design nonlinear-optical devices based on Λ-type configurations in N-V centers.

We have performed spectral hole-burning experiments on a diamond sample with very little inhomogeneous broadening in order to gain a better understanding of the excited-state structure. The sample was a type 1b high-temperature, high-pressure (HPHT)-grown crystal obtained originally from Sumitomo. Fig. 4 shows a photoluminescence image of the sample. The bright squares are from regions deliberately implanted with 2MeV He at a fluence of $\sim 10^{17}$ cm^{-2}. Annealing combines damage (vacancies) with the residual N to create N-V centers, but there is also formation of N-V centers within the nominally unimplanted regions, due to residual vacancies combining with N, and also vacancies caused by the act of imaging the sample with the Focussed Ion Beam (FIB). Although the N occurs throughout the crystal, most of the luminescence comes from close to the surface, as only the surface N has been converted to N-V as the vacancy concentration is greatest near the surface (due to the imaging and implantation).

Another important feature that can be seen in Fig 4 is the presence of distinct sectors. Growth sectors are regions that have grown from different faces of the original seed crystal. Because different faces grow at different rates, and incorporate impurities at different levels, the sample shows marked discontinuities at the boundaries between different sectors. In particular growth sectors the inhomogeneous linewidth of the NV$^-$ zero-phonon line (ZPL) at 637 nm was exceptionally narrow, approximately $10 - 20$ GHz, which should be compared with the generally accepted value of 750 GHz.[31] These growth sectors are outlined in the figure. The photoluminescence linewidth changes abruptly at the boundaries of these sectors but changes little within the sectors. Our interpretation is that these sectors grew along a particular orientation for which the impurity concentration rate during growth is low. The heavily-implanted regions have severely broadened ZPLs, but they

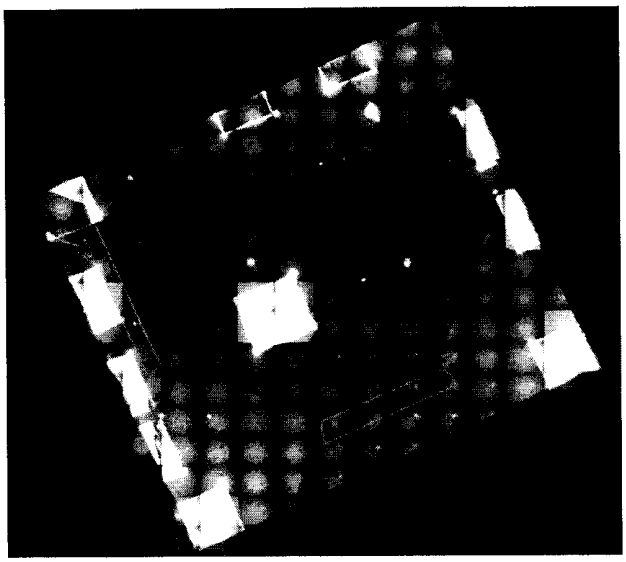

Figure 4. Fluorescence image of the diamond sample. This is a mosaic made from many smaller images (the small tiles). In each tile, the sample was excited by a defocused laser beam (532 nm wavelength, and the fluorescence was collected with a 10x microscope objective. Reflected laser light was removed using an edge filter with a cutoff wavelength close to 532 nm.

produce strain that extends into the surrounding regions. Since one of the heavily-implanted regions is adjacent to a narrow-linewidth sector, the effect of strain on a narrow ZPL can be observed.

Fig. 5 shows the experimental setup used for the two-laser measurements. The sample was cooled to approximately 10 K in a liquid-helium continuous-flow cryostat. Two beams from independently tunable external-cavity diode lasers operating near 637 nm were combined on a beamsplitter. These were then combined on another beamsplitter with a beam from a 532 nm solid-state laser. The combined beams were inserted into the collection path using a third beamsplitter, and then focused through a thin cryostat window onto the diamond sample using a microscope objective (0.6 numerical aperture) with adjustable cover-slip correction that provided nearly diffraction-limited imaging. However, in this experiment the lasers were focussed to spots with diameters of approximately 3 μm. The collected fluorescence was first passed through an edge filter to remove the back-reflected laser light, and was then sent either to a cooled-CCD spectrometer for ordinary photoluminescence measurements, or to an avalanche-photodiode photon counter (Perkin-Elmer SPCM) for photoluminescence excitation (PLE) or spectral hole-burning measurements. Before the photon counter, the collected light was filtered by a bandpass filter centered at 700 nm with a 40 nm bandwidth in order to select fluorescence from a portion of the phonon sidebands. The electronic pulses from the photon counter were recorded by a Picoquant TimeHarp card operating with a router in time-tagged mode. A portion of the output from the two scanning lasers was also sent to a pair of scanning Fabry-Perot cavities having free spectral ranges of 30 GHz and 300 MHz. These were used to monitor laser operation. For some of the measurements, the 300 MHz cavity was held fixed so that the photodiode produced a pulse each time the scanning laser crossed a cavity resonance. These pulses were converted into TTL pulses and recorded by the Picoquant card along with the photon counter events, providing an accurate frequency calibration.

Fig. 6a shows a photoluminescence spectrum obtained at a temperature of 10 K in one of the narrow-linewidth regions under 532 nm excitation. The ZPL is split into two orthogonally-polarized components by strain, and the individual components are not much wider than the spectrometer resolution (0.02 nm). A corresponding PLE measurement is shown in Fig. 6b. This measurement was performed by scanning one of the external-cavity diode lasers in frequency across the ZPL while monitoring fluorescence into the phonon sidebands. As

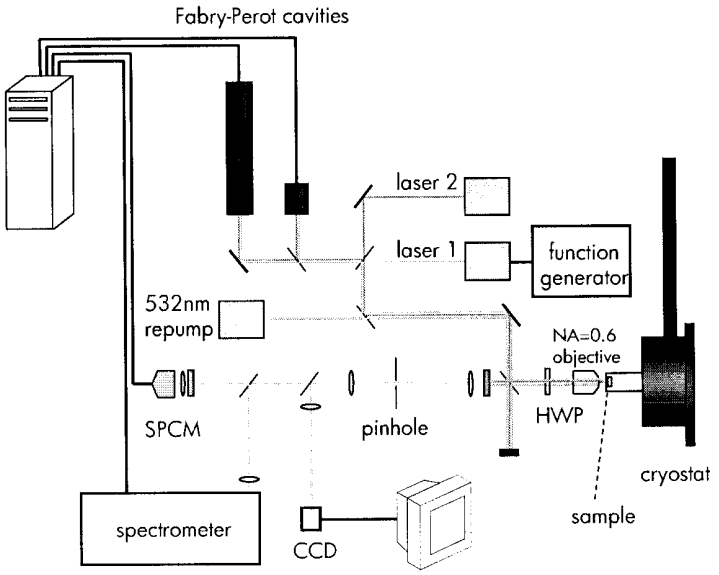

Figure 5. Simplified diagram of the experimental setup.

in the photoluminescence measurement, two orthogonally polarized peaks are observed. Each component is approximately 15 GHz wide. Interestingly, in the PLE measurement, the longer-wavelength peak is much smaller than the shorter-wavelength peak, while in the nonresonant photoluminescence measurements, the two peaks have approximately equal area. Our interpretation of this is that a strong optical pumping effect occurs in the longer-wavelength peak under resonant excitation. This is consistent with the spectral-hole burning results presented below. A variety of strain conditions can be studied on this sample, and photoluminescence and PLE results from several locations are shown in Fig. 7. Spectra containing a single narrow line, two orthogonally-polarized components, three peaks, and four peaks have all been observed.

In the above spectra, despite the narrow inhomogeneous linewidth, the fine structure is still hidden. The fine structure can be revealed in two-laser spectral hole-burning measurements.[28,29] This is possible because the fine structure splitting within the ground and excited states varies much less than the ground-to-excited-state spacing. Two examples of such measurements are shown in Fig. 8. Here, excited state fluorescence is measured as a function of detuning between two excitation lasers. A series of peaks, or "antiholes," is observed. These correspond to particular detunings for which each laser excites a transition involving a different ground state. The enhanced fluorescence occurs in such cases because the two lasers cooperate to excite a particular subset of the N-V centers no matter which ground state they are in. On the other hand, if only one laser is on resonance with a transition, after a few fluorescence cycles it will drive the population to whichever ground state it cannot excite (optical pumping). This argument assumes that the excited state has a finite probability to relax to this other ground state. Otherwise, no optical pumping effect would be observed. The two plots in Fig. 8 were measured at the same location as the photoluminescence and PLE spectra shown in Fig. 6, where the ZPL is split by strain into two peaks. The polarization was rotated approximately 45° relative to axes along which the two ZPL components are polarized. Fig. 8a was measured on the long-wavelength peak, while Fig. 8b was measured on the short-wavelength peak. While the long-wavelength peak was much smaller than the short-wavelength peak in the PLE measurements, the heights of the antiholes are similar, and the contrast ratio is much better for the long-wavelength peak. This is further evidence that optical pumping plays an important role when the the long-wavelength peak is excited on resonance.

The antihole features are shown in more detail in Fig. 9. The peaks at ± 2.88 GHz correspond to the ground-state level spacing. It is known from previous experiments that the ground-state structure varies little with

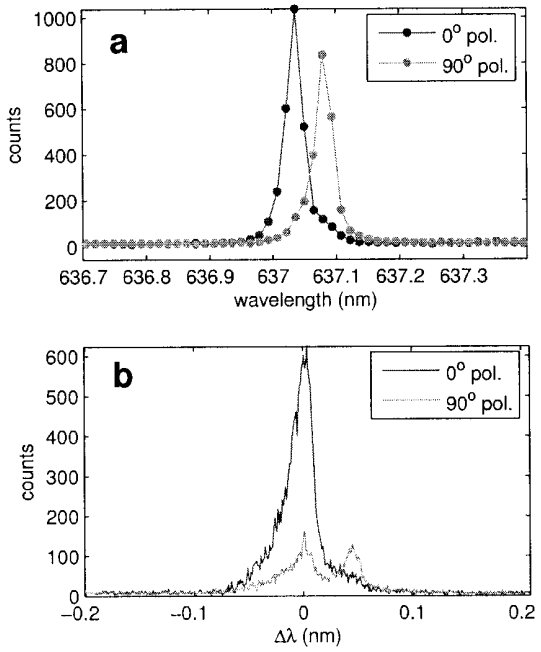

Figure 6. (a) Photoluminescence spectra under 532 nm excitation, measured at a location where the zero-phonon line is split into two peaks. The red curve (long-wavelength peak) was measured for the excitation and collection polarization parallel to the edge of the nearby implanted region, while the blue curve (short-wavelength peak) was measured for the excitation and collection polarization perpendicular to the edge of the implanted region. (b) Photoluminescence excitation spectra measured at the same location, with the same two polarizations.

strain.[32] The existence of these peaks shows that one or more of the excited state has a nonzero transition strength to both ground states. The other antihole features correspond to cases where the two ground states are excited to two different excited states by the two lasers. The locations of these antiholes can be used to construct a possible level diagrams corresponding to each transition, as shown in the figure. We consider only three excited states, as was done in Ref. 29.

In Fig. 10, the antihole patterns are compared for the long- and short-wavelength components of the ZPL. The peaks at ±2.88 GHz are much stronger for the long-wavelength component, indicating that the non-spin-preserving transition is much stronger in this case. This may also explain why the optical pumping effect appears much stronger for the long-wavelength component, since the efficiency of optical pumping depends on the strength of the non-spin-preserving relaxation. The excited-state fine structure is apparently very different for the two strain-split components of the ZPL.

A strain dependence of the excited-state fine structure can be seen in the long-wavelength component of the ZPL line as the sample position is varied. Fig. 11 shows how the two-laser spectrum changes with position, beginning at the edge of an implanted region (top) and then moving away. A continuous change in the antihole positions and intensities is observed. Most interestingly, the antiholes at ±2.88GHz become strongest as two neighboring antiholes approach from either side. These two neighboring antiholes are quite unequal in intensity when they are far from the 2.88GHz antihole, but when they are close, the intensities become approximately equal. This behavior appears consistent with an anticrossing behavior occurring in two of the excited states as the strain is varied. When the two satellite peaks have equal heights, there are two closely spaced excited levels that couple in the same way to the ground levels.

In summary, our spectroscopic results indicate that the optical transitions in N-V centers are generally not spin-preserving. The strong antihole features at two-laser detunings of ±2.88 GHz indicate that it should be

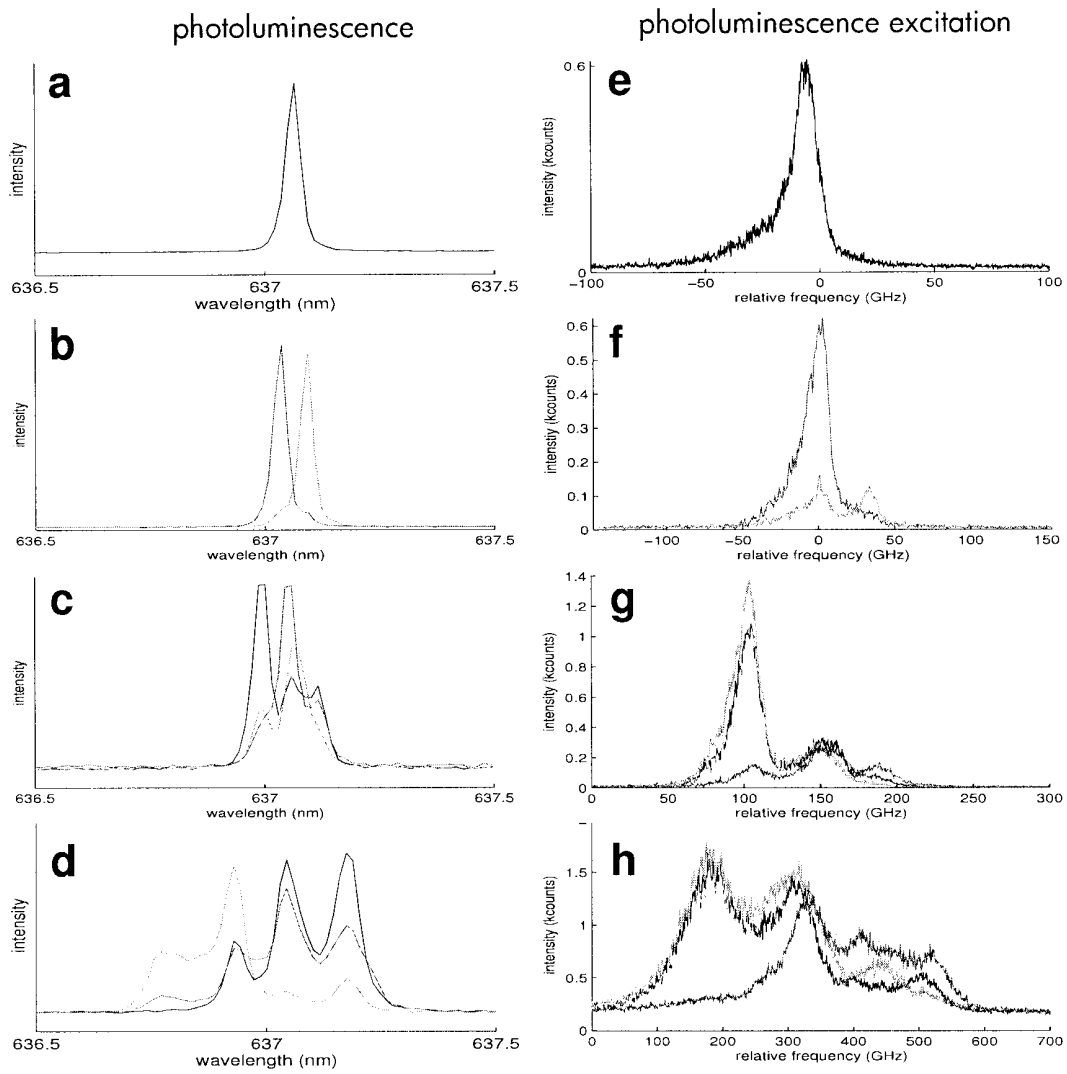

Figure 7. (a) Photoluminescence (PL) spectrum under 532 nm excitation at a location where the zero-phonon line does not show splitting. In this case, the emission had very little polarization dependence. (b) PL spectrum at a location where the zero-photon line is split into two peaks, measured for two orthogonal polarizations, as in Fig.6. (c) PL spectrum at a location with three peaks measured for four different polarizations 0°, 45°, 90°, and 135° relative to a specially chosen direction. (d) Similar measurements at a location with four peaks. (e-h) Photoluminescence excitation measurements at the same four locations, and with the same polarizations, as in the corresponding photoluminescence spectra.

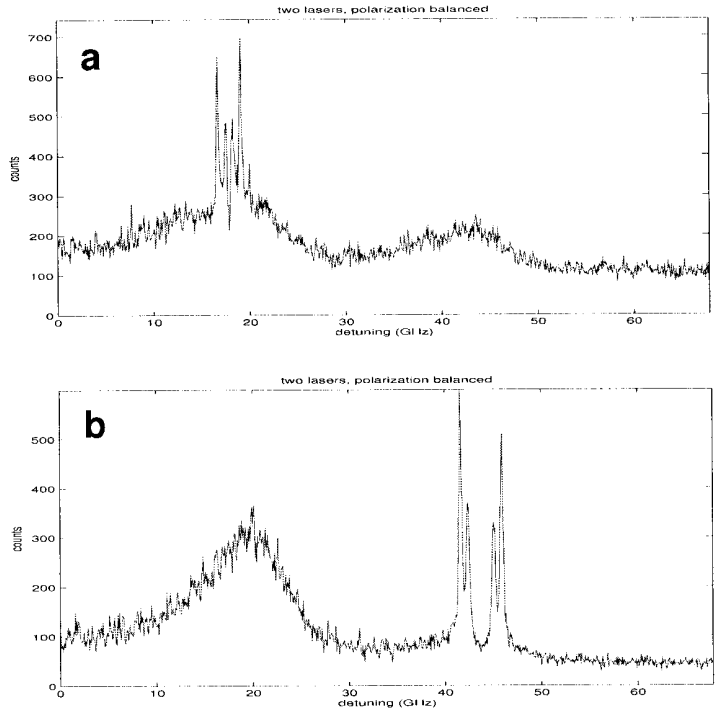

Figure 8. Two-laser measurements with fixed laser centered on (a) the short-wavelength peak and (b) the long-wavelength peak from Fig. 6. The same excitation polarization was used in both cases, oriented approximately 45° degrees relative to the axes along which the two peaks are polarized.

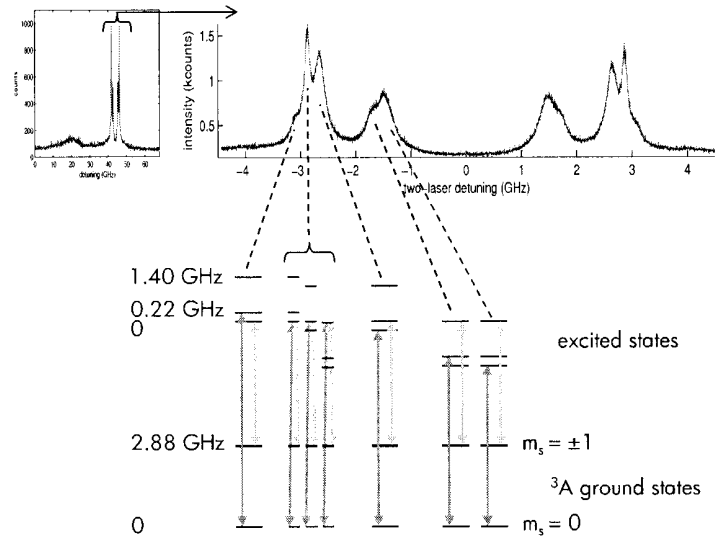

Figure 9. Two-laser measurement with fixed laser centered on the long-wavelength peak from Fig. 6. Energy-level diagrams explaining each peak on the left side of the spectrum are given. The separations between the ground and excited manifolds vary due to inhomogeneous broadening.

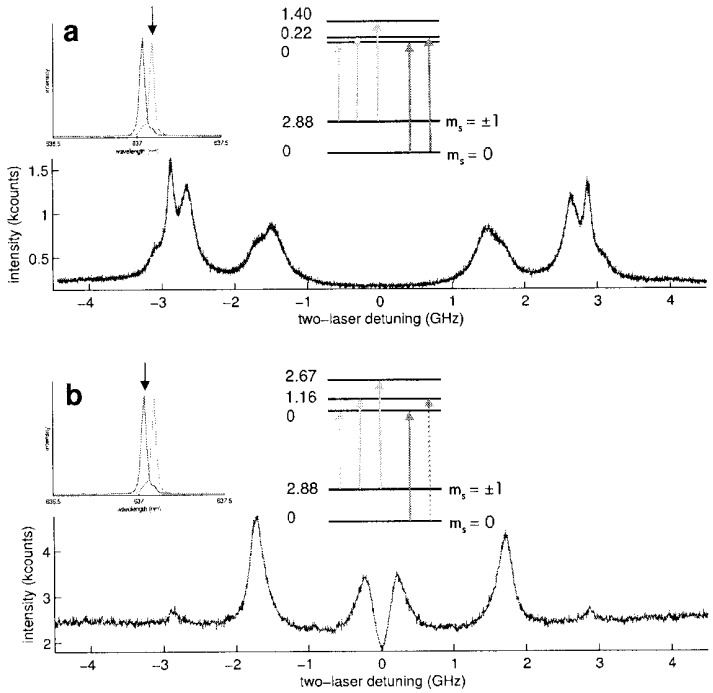

Figure 10. High-resolution two-laser measurements with fixed laser centered on (a) the long-wavelength peak from Fig. 6 and (b) the short-wavelength peak. Energy-level diagrams that can explain the observed features are given in each case. The dotted lines indicate transitions that must be almost forbidden, based on the weak antihole features at ±2.88 GHz.

possible to isolate a good Λ system even at zero magnetic field involving all four orientations of N-V centers at once if desired. Furthermore, based on the data and inferred level diagram shown in Fig. 9, it appears that a four-level N system can be realized. The $m_s = 0$ and $m_s = \pm 1$ ground levels both connect to either of the two lowest excited states, and the $m_s = \pm 1$ level also connects to the upper excited state. We therefore hope to use this physical system for the realization of the 4-state quantum non-demolition device described above.

Acknowledgments

We acknowledge K. Nemoto, S. D. Barrett and P. Kok for contributions to the parity gate and Bell state analyzer ideas discussed above. The work performed at HP Laboratories in Palo Alto has been supported in part by DARPA contract no. FA9550-05-C-0017. Quantum Communications Victoria is supported by the State Government of Victoria's Science, Technology and Innovation Initiative - Infrastructure Grants Program. BCG is proudly supported by the *International Science Linkages* programme established under the Australian Government's innovation statement *Backing Australia's Ability*. This work was supported by the DEST, Australian Research Council, the Australian government and by the US National Security Agency (NSA), Advanced Research and Development Activity (ARDA) and the Army Research Office (ARO) under contracts W911NF-04-1-0290 and W911NF-05-1-0284.

REFERENCES

1. G. J. Milburn, "Quantum optical Fredkin gate" *Phys. Rev. Lett.*, **62**, 2124-2127, 1987.
2. E. Knill, L. Laflamme, and G. J. Milburn, "A scheme for efficient quantum computation with linear optics" *Nature (London)* **409**, 46-52, 2001.

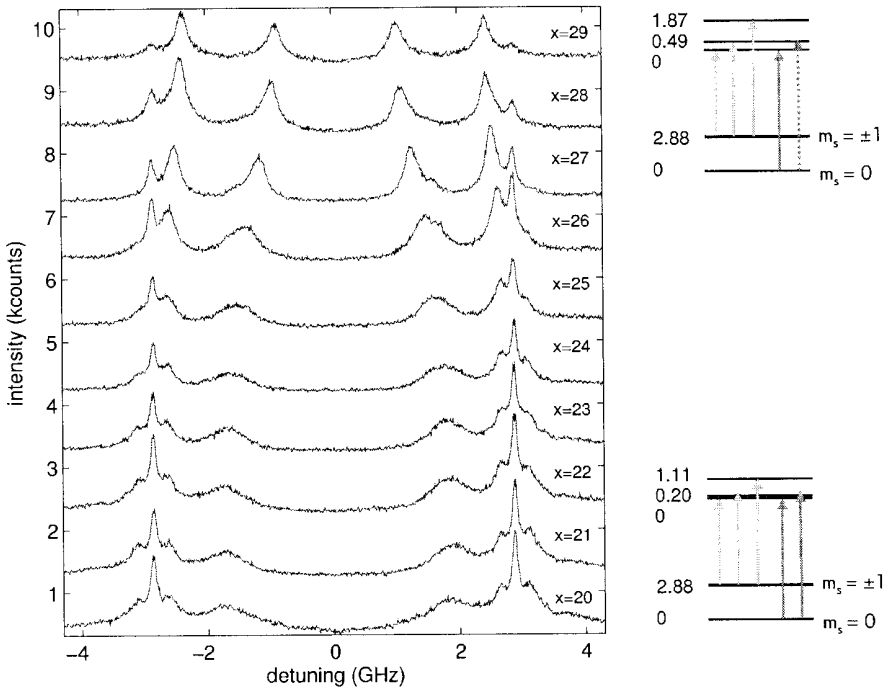

Figure 11. Position dependence of antihole pattern measured on the long-wavelength component of the zero-phonon line. The curve on the top was measured right next to a heavily implanted region. The distance increases by 10 μm for each step. Possible energy level diagrams corresponding to the antihole patterns in the first and last curves are shown on the right.

3. F. Jelezko, I. Popa, A. Gruber, C. Tietz, J. Wrachtrup, A. Nizovtsev and S. Kilin, "Single spin states in a defect center resolved by optical spectroscopy," *Appl. Phys. Lett.* **81**, pp. 2160–2162 (2002).
4. E. A. Wilson, N. B. Manson and C. Wei, "Perturbing an electromagnetic induced transparency within an inhomogeneously broadened transition," *Phys. Rev. A* **67**, pp. 023812-1–10 (2003).
5. A. Beveratos, S. Kühn, R. Brouri, T. Gacoin, J-P Poizat, and P. Grangier P, "Room temperature stable single-photon source", *European Physical Journal D* **18**, 191, 2002.
6. J. R. Rabeau, S. T. Huntington, A. D. Greentree, and S. Prawer, "Diamond chemical vapour deposition on optical fibres for fluorescence waveguiding", *Appl. Phys. Lett.* **86**, 134104, 2005.
7. A. D. Greentree, J. Salzman, S. Prawer, and L. C. L. Hollenberg, "Quantum gate for Q switching in monolithic photonic bandgap cavities containing two-level atoms", to appear in *Phys. Rev. A* , quant-ph/0511107.
8. L. Childress, J. M. Taylor, A. S. Sorensen and M. D. Lukin, "Fault-tolerant quantum repeaters with minimal physical resources and implementations based on single-photon emitters," *Phys. Rev. A* **72**, pp. 052330-1–16 (2005).
9. A. P. Nizovtsev, S. Ya. Kilin, F. Jelezko, T. Gaebal, I. Popa, A. Gruber and J. Wrachtrup, "A quantum computer based on NV centers in diamond: optically detected nutations of single electron and nuclear spins," *Opt. Spectrosc.* **99**, pp. 233–244 (2005).
10. M. S. Shahriar, P. R. Hemmer, S. Lloyd, P. S. Bhatia, and A. E. Craig, "Solid-state quantum computing using spectral holes," *Phys. Rev. A* **66**, 032301 (2002).
11. P. Olivero, S. Rubanov, P. Reichart, B. Gibson, S. Huntington, J. Rabeau, A. D. Greentree, J. Salzman, D. Moore, D. N. Jamieson, S. Prawer, "Ion Beam Assisted Lift-Off Technique for Three-Dimensional Micromachining of Free Standing Single-Crystal Diamond", *Advanced Materials*, **17**, 2427-2430, 2005.

12. A. D. Greentree, P. Olivero, M. Draganski, E. Trajkov, J. R. Rabeau, P. Reichart, B. C. Gibson, S. Rubanov, S. T. Huntington, D. N. Jamieson, and S. Prawer, "Critical components for diamond-based quantum coherent devices", preprint.
13. P. R. Hemmer, A. V. Turukhin, M. S. Shahriar and J. A. Musser, "Raman-excited spin coherences in nitrogen-vacancy color centers in diamond," *Opt. Lett.* **26**, pp. 361–363 (2001).
14. R. G. Beausoleil, W. J. Munro, and T. P. Spiller, "Applications of coherent population transfer to quantum information processing," *J. Mod. Opt.* **51**, pp. 1159–1601, 2004.
15. R. G. Beausoleil, W. J. Munro, D. A. Rodrigues, and T. P. Spiller, "Applications of electromagnetically induced transparency to quantum information processing," *J. Mod. Opt.* **51**, pp. 2441–2447, 2004.
16. W. J. Munro, K. Nemoto, R. G. Beausoleil, and T. P. Spiller, "High-efficiency quantum nondemolition single-photon-number-resolving detector," *Phys. Rev. A* **71**, p. 033819, 2005.
17. N. Imoto, H. A. Haus, and Y. Yamamoto, "Quantum nondemolition measurement of the photon number via the optical kerr effect," *Phys. Rev. A* **32**, pp. 2287–2292, 1985.
18. S. E. Harris, J. E. Field, and A. Imamoglu, "Nonlinear optical processes using electromagnetically induced transparency", *Phys. Rev. Lett.* **64**, 1107-1110, 1990.
19. H. Schmidt and A. Imamoğlu, "Giant kerr nonlinearities obtained by electromagnetically induced transparency," *Opt. Lett.* **21**, pp. 1936–1938, 1996.
20. P. Grangier, J. A. Levenson, and J.-P. Poizat, "Quantum non-demolition measurements in optics," *Nature* **396**, pp. 537–542, 1998.
21. J. C. Howell and J. A. Yeazell, "Nondestructive single-photon trigger," *Phys. Rev. A* **62**, p. 032311, 2000.
22. S. D. Barrett, P. Kok, K. Nemoto, R. G. Beausoleil, W. J. Munro, and T. P. Spiller, "Symmetry analyzer for nondestructive Bell-state detection using weak nonlinearities," *Phys. Rev. A* **71**, p. 060302, 2005.
23. J. Preskill, "Reliable quantum computers", *Proc. R. Soc. London Ser. A* **454**, 385-410, 1998.
24. W. J. Munro, K. Nemoto, T. P. Spiller, S. D. Barrett, P. Kok, and R. G. Beausoleil, "Efficient optical quantum information processing," *J. Opt. B: Quant. Semiclass. Opt.*, **7**, pp. S135–S140 (2005).
25. W. J. Munro, K. Nemoto, and T. P. Spiller, "Weak nonlinearities: a new route to optical quantum computation," *New J. Phys.*, **7**, pp. 137–148 (2005).
26. K. Nemoto and W. J. Munro, "Nearly Deterministic Linear Optical Controlled-NOT Gate," *Phys. Rev. Lett.* **93**, p. 250502, 2004.
27. T. P. Spiller, K. Nemoto, S. L. Braunstein, W. J. Munro, P. van Loock, and G. J. Milburn, "Quantum Computation by Communication," *arXiv:quant-ph/0509202*, 2005.
28. N. R. S. Reddy, N. B. Manson and E. R. Krausz, "Two-laser spectral hole burning in a colour centre in diamond," *J. Luminescence* **38**, pp. 46–47 (1987).
29. N. B. Manson and C. Wei, "Transient hole burning in N-V center in diamond," *J. Luminescence* **58**, pp. 158–160 (1994).
30. G. Davies and M. F. Hamer, "Optical studies of the 1.945 eV vibronic band in diamond", *Proc. R. Soc. London Ser. A* **348**, 285-298, 1976.
31. Zaitsev AM 2001 "Optical Properties of Diamond: A Data Handbook", (Berlin: Springer)
32. E. van Oort, B. van der Kamp, R. Sitters, and M. Glasbeek, "Microwave-induced line-narrowing of the N-V defect absorption in diamond," *J. Luminescence* **48 & 49**, 803 (1991).